A constitutive equation for fiber-reinforced masonry arches

M. Lucchesi, B. Pintucchi and N. Zani
University of Florence, Department of Constructions, Florence, Italy

ABSTRACT: A numerical model for analyzing fiber-reinforced masonry arches is presented. It is based on a constitutive equation formulated for one-dimensional masonry elements, assumed to be made of a non-linear elastic material with no resistance to tension and limited compressive strength. The reinforcement, which is instead assumed to have no resistance to compression and limited tensile strength, is applied on the inner and/or outer side of the arch. In order to capture any possible FRP debonding, a procedure is then developed to predict the values of the tangential and normal interactions between the masonry and the fiber. The model, implemented into a FEM computer code, allows for short computational times in studying reinforced masonry arches with any geometries, restraints and loading conditions. Preliminary comparisons with experimental results are carried out to verify the effectiveness and accuracy of the model's predictions.

1 INTRODUCTION

In recent years, specialists have increasingly sought to address the problems inherent in reinforcing masonry structures. This is for a number of reasons. Firstly, there is a growing need to preserve the architectural identities of masonry buildings – their aesthetic and historical value. Moreover, a number of earthquakes have revealed the seismic vulnerability of such structures. Lastly, the models and calculation techniques used so far have proved incapable of accurately predicting the complex behavior of masonry, thus highlighting the need for further research.

Recently, modern materials technology has provided new possibilities through light and removable retrofit techniques utilizing efficient and easily worked reinforcing components. In this respect, fiber reinforcement techniques have been adopted successfully to restore many masonry structures (Bakis et al. 2002). Nevertheless, research efforts are still needed to fully comprehend the structural behavior of arches, and more in general masonry buildings, strengthened with Fiber Reinforced Plastic composites (FRP). In recent years, the foregoing reasons have prompted many authors to seek behavioral models and numerical procedures able to predict their structural response (Luciano et al. 2002, Ascione et al. 2005, Drosopoulos et al. 2007).

In previous works, we defined a numerical model for performing non-linear static and dynamic analyses of masonry columns, arches, towers and slender structures, in general. Based on such results, in this paper we present a simple model for fiber-reinforced masonry elements. To this end, a constitutive equation has been developed to model one-dimensional elements made of a non-linear elastic material, with no resistance to tension and limited compressive strength. The reinforcement, which is instead assumed to have no resistance to compression, is applied to the intrados and/or extrados of the arches. Limited tensile strength can also be considered for the FRP, though such a premise is less profitable from a practical standpoint.

Furthermore, a simple procedure has been developed to determine the normal and tangential interactions between the arch and the reinforcement, the aim being to monitor if and when FRP

debonding might occur. In this respect, it is worthwhile noting that post-debonding analyses are not possible with the current version of the model, though this issue is currently under investigation and will be the topic of a forthcoming paper.

2 MODEL SPECIFICATIONS

2.1 Constitutive equation

By presuming that the sections remain plane and orthogonal to the line of the deformed axis, and accounting for axial stress alone, the deformation of a beam can be described in terms of two generalized strains only: extensional strain ε and curvature κ of the axis. Under the aforementioned assumptions, the behavior of both masonry and the reinforcement material can be described as in figure 1, where σ_c and ε_c (Fig. 1a) respectively denote the minimum admissible compressive stress and the strain at which such stress is first attained in the masonry. For fibers applied to the intrados and the extrados, the maximum admissible tensile stress and the corresponding strain are indicated in figure 1b) as σ_i, σ_e and ε_i, ε_e, respectively (where the subscripts *i* and *e* stand for intrados and extrados). Such distinction has been made to render the model as general as possible, so that, for example, it can also be used to represent the common cases of reinforcement on the extrados or intrados alone. In the same way, the geometrical and other mechanical properties will hereafter be specified in general terms, by means of the subscripts *i* and *e*, depending on FRP location.

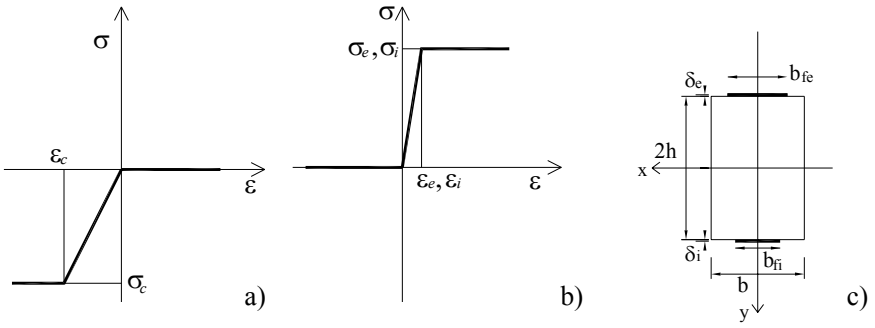

Figure 1 : σ-ε diagram under uniaxial stress for a) masonry, b) reinforcement material; c) section's geometry.

The amounts of exterior and interior reinforcement in a given cross-section are taken into account, respectively, through the two parameters K_e and K_i:

$$K_e = n_e E_e \delta_e, \quad K_i = n_i E_i \delta_i, \tag{1}$$

where, as shown in figure 1c), δ_e, δ_i represent the composite fiber thickness, $n_e = b_{fe}/b$ $n_i = b_{fi}/b$ denote the width of the composites normalized to the section width *b,* and E_e and E_i are their Young's modulus.

As a consequence of the above kinematic and constitutive assumptions, the diagram of the axial stress σ, in a generic rectangular cross section of dimensions *b* and *2h,* reinforced on both the intrados and extrados, is one of those presented in Fig. 2, which illustrates the cases for $\kappa<0$ alone.

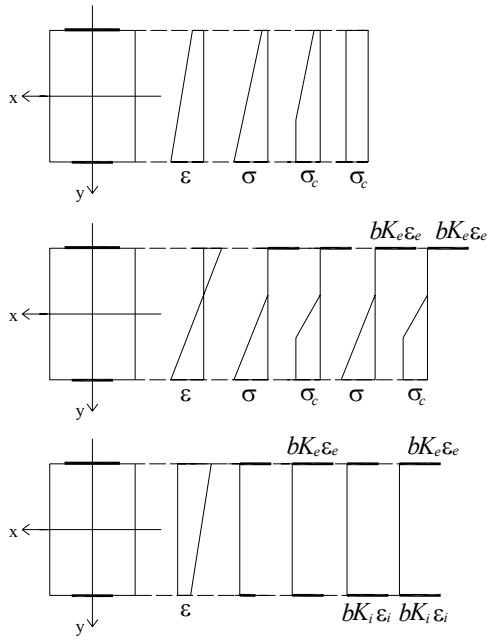

Figure 2 : ε and σ patterns over a generic cross-section.

In all cases, the normal stress σ has a piecewise linear diagram. Let y_1, y_2, y_3, y_4 be the positions where σ reaches the values 0, σ_c σ_e and σ_i, respectively. Their values can be easily expressed as functions of ε and κ, from equations

$$\varepsilon(y_1)=\varepsilon+\kappa y_1=0,\quad \varepsilon(y_2)=\varepsilon+\kappa y_2=\varepsilon_c,\quad \varepsilon(y_3)=\varepsilon+\kappa y_3=\varepsilon_e,\quad \varepsilon(y_4)=\varepsilon+\kappa y_4=\varepsilon_i \tag{2}$$

which are a consequence of the Euler-Bernoulli hypothesis.
Consequently, the plane of generalized strains turns out to be naturally divided into 22 regions, in each of which the above stress regimes hold. In this way, the constitutive relation, i.e. the mapping which associates the corresponding generalized stress to the generalized strain, the axial force N and the bending moment M can all be determined.

To this end, it is convenient to introduce the following non-dimensionalized parameters:

$$\eta=\frac{\varepsilon}{\varepsilon_c},\quad \chi=\frac{\kappa h}{\varepsilon_c},\quad n=\frac{N}{2bh\sigma_c},\quad m=\frac{M}{2bh^2\sigma_c},\quad k_e=\frac{K_e\varepsilon_c}{2h\sigma_c},\quad k_i=\frac{K_i\varepsilon_c}{2h\sigma_c}. \tag{3}$$

Although the model has been developed to provide for a limit to FRP tensile strength in view of future enhanced behavioral representations, for the sake of brevity, the general case has been left out here, as FRP's limited strength to tension actually only comes into play in a rather limited number of cases. Therefore, in the following we refer to reinforcement with unlimited tensile strength as a special case of the composite's assumed behavioral law, shown in Fig. 1b), that is, for $\sigma_i\to\infty$ and $\sigma_e\to\infty$.

Under such circumstances, the partition in the (η,χ) plane is reduced to the six plus six regions shown in Fig. 3 – symmetrical with respect to the η axis – in which the following relations hold:

$$
\begin{aligned}
&\Sigma_1 : n = \eta, \quad m = \chi; \\
&\Sigma_2 : n = -\frac{\chi^2 - 2\chi(\eta+1) + (\eta-1)^2}{4\chi}, \quad m = \frac{2\chi^3 + 3\chi^2(1-\eta) + (\eta-1)^3}{4\chi^2}; \\
&\Sigma_3 : n = 1, \quad m = 0; \\
&\Sigma_4 : n = \frac{(\eta+\chi)^2}{4\chi} + k_e(\eta-\chi), \quad m = \frac{-\eta^3 + 3\chi^2\eta + 2\chi^3}{4\chi^2} + 3k_e(\chi-\eta); \\
&\Sigma_5 : n = \frac{2\eta - 1 + 2\chi}{4\chi} + k_e(\eta-\chi), \quad m = \frac{-3\eta^2 + 3\eta - 1 + 3\chi^2}{4\chi^2} + 3k_e(\chi-\eta); \\
&\Sigma_6 : n = \chi(k_i - k_e) + \eta(k_i + k_e), \quad m = 3\left[\chi(k_i + k_e) + \eta(k_i - k_e)\right].
\end{aligned}
\tag{4}
$$

Similar relations can be obtained for regions Σ'_i (i=1,..,6) by virtue of simple symmetrical properties.

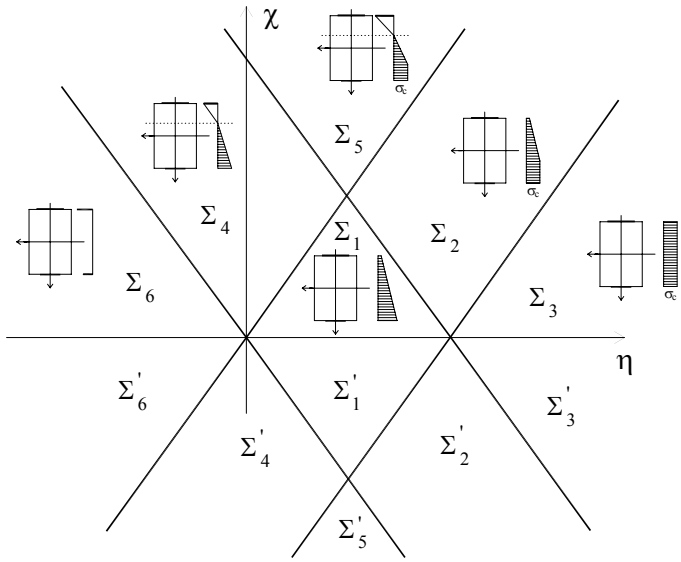

Figure 3 : Partition of the plane (η,χ).

2.2 Finite element model

Despite the relative simplicity of the proposed constitutive relation, explicit solutions to equilibrium problems of reinforced masonry arches are nonetheless very difficult to obtain and generally require resorting to numerical methods.

To this end, a finite element approach has been followed. In particular, in discretizing the one-dimensional structures into finite elements: i) three degrees of freedom – axial and transverse displacements plus rotation – have been assigned at each node; ii) conforming elements and Hermite shape functions have been selected to guarantee the continuity of both transverse displacements and rotations; iii) linear shape functions have been used for axial displacements, as well. In addition, standard numerical techniques, based on the Newton-Raphson iterative method, have been used to solve the non-linear system resulting from the structure's discretization. Note that this method requires explicit evaluation of the derivatives of the generalized stresses given in Eq. (4) with respect to the generalized strains.

The numerical method has been implemented into a finite element code, which enables analyzing both unreinforced and reinforced arches, with any geometries and restraints, under any loading conditions, together with their self-weight.

2.3 Failure modes

To date, a great deal of research has been devoted to identifying the modes of collapse of masonry arches, most of which are widely recognized. The first is the classical four/five hinges mechanism studied by Heyman (1982), which is typical of unreinforced arches subjected to a vertical pointwise load. Such a collapse mode is attributed to masonry's low or null tensile strength.

Less widespread, and consequently less well-known, are cases of failure that actually involve masonry crushing. If a limited compressive strength is accounted for, under some particular loading conditions, hinges may occur upon collapse of unreinforced arches, not only with masonry cracking, but crushing as well (Lucchesi et al. 1996, Pintucchi and Zani 2007). A similar failure mode, termed compressive crushing, may also be exhibited by FRP-strengthened arches, as the reinforcement prevents or at least reduces the cracking of sections.

The proposed model is able to predict both these failure modes, together with the corresponding ultimate load, as both masonry's inability to furnish tensile strength and its bounded compressive strength are embedded into the constitutive equation, which provides for cracking and crushing of the masonry. In this respect, it should however be noted that, in contrast to what generally occurs in unreinforced arches undergoing compressive failure, the model predicts that crushing failure in FRP-strengthened arches occurs at rather high strain values, due to the low location of the neutral axis in the section caused by the presence of the reinforcement. Therefore, analyzing such structures calls for setting a limit value to compressive deformability.

Experimental tests performed in recent years have shed light on other phenomena that may affect the load carrying capacity of a reinforced arch, as well as the mechanisms governing collapse. If reinforcement is applied to the intrados of an arch, when the connection between the FRP and the masonry is poor, debonding of the FRP may occur, considerably decreasing its strengthening effects. Moreover, experimental evidence shows that an arch may also collapse because the masonry stones slide at the springings and at the point of concentrated loading, especially when the reinforcement is applied along the entire length of the extrados (Drosopoulos et al. 2007).

Such possible premature collapse modes cannot be provided for directly in the proposed model. However, monitoring the possible onset of the earliest debonding phenomena can be conducted by estimating the values of the FRP-masonry interactions with increasing applied load. Indeed, debonding is certainly related to the values at the masonry-composite interface of normal (peeling) stress and shear stress, here respectively referred to as σ_{rad} and τ_{tan}. Such values can be easily obtained through equilibrium considerations, once the axial force N_f in the reinforcement has been determined. In fact, the reinforcement may be interpreted simply as a circular arch subjected to axial force alone, in equilibrium with the distributed tangential and radial load, p and q, which result from both the arch's actions on the composite and any eventual external loads.

As the bending moment and the shear force in the fiber are null, the equilibrium equations of a circular arch of radius r_f are:

$$q = -\frac{dN_f}{ds}, \quad p = -\frac{N_f}{r_f}, \tag{5}$$

where s is the natural parameter. Therefore, we have

$$\tau_{\tan} = -\frac{1}{b_f}\frac{dN_f}{ds}, \quad \sigma_{rad} = -\frac{N_f}{b_f r_f}, \tag{6}$$

where b_f is the width of the composite fiber.

As debonding generally coincides with failure of a masonry layer close to the interface, rather than failure of FRP's adhesive power, the following criterion seems to be appropriate (Triantafillou, 1998):

$$\frac{\sigma_{rad}}{2} + \sqrt{\frac{\sigma_{rad}^2}{4} + \tau_{\tan}^2} = f_b. \tag{7}$$

Of course, this approach requires knowing the limiting value, $f_{b,lim}$, of f_b, related to debonding and precludes post-debonding analysis.

Although not considered herein, the sliding of sections could be checked via a similar procedure, by predicting the shear stress in comparison with a bounded reference value.

3 CASE STUDIES

In this section we evaluate some case studies to check the proposed model's ability to effectively predict the ultimate load and failure modes of reinforced and unreinforced arches. The numerical study is carried out with reference to arches whose behavioral response up to collapse has been recently determined through experimental tests. For the purposes of comparison, some of the available results are presented in Briccoli Bati and Rovero (2000) and Briccoli Bati et al. (2004).

In this preliminary study, comparisons with experimental data have been useful chiefly to verify the model's ability to capture the actual collapse mechanisms of tested specimens, especially from a qualitative perspective. An attempt has also been made to infer the reference limiting value, $f_{b,lim}$, in order to avoid premature FRP detachment. Moreover, we have also focused our attention on identifying a reasonable bound for masonry's deformability under compression, ε_m, referred to in the following as $\varepsilon_{m,lim}$.

The analyzed structure is a reduced circular arch with clamped springings and mean radius r = 91.5 cm, a uniform rectangular cross-section of dimensions $b = h$ = 10 cm, and springing angle Θ equal to 30° (Fig. 4). It is subjected to the pointwise load P, which is increased until collapse occurs.

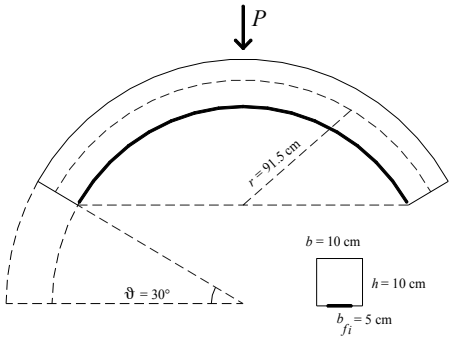

Figure 4 : Analyzed arch.

The analyzed arch is considered both in the unreinforced version (Case A), and with a reinforcement attached to the entire intrados. The mechanical properties assumed for the masonry and composite fibers are listed in Table 1.

Table 1 : Masonry and FRP properties

	γ (kg/m^3)	E (MPa)	σ_c (MPa)	σ_i (MPa)	δ_i (mm)
Brick	1800	1785	17.39		
Mortar	200	133	7.8		
Masonry	1800	830	8.6		
MBrace Fibers C1-130	1820	230000		> 3430	0.176
primer	1067	> 700		> 12	
adhesive	1020	> 3500		> 50	
Composite		31545			0.08

Four variants of the FRP-strengthened arch (Cases B, C, D, E) have been considered by varying the reinforcement fiber width b_f, from 10 cm to 1.25 cm.

Table 2 shows the collapse load values reported in the aforementioned experimental study for

each of the considered cases, which also revealed different failure modes. The unreinforced arch (Case A) undergoes the classical five-hinge collapse mechanism, ascribable to masonry's low tensile strength. In the other cases, FRP debonding and compressive masonry failure occur, depending on the reinforcement width. More precisely, Case B, with the smallest amount of FRP, is characterized by premature detachment of the FRP, followed by a failure mode similar to the unreinforced arch; in Case C, progressive debonding takes place, accompanied by the onset of masonry crushing at the keystone. Finally, in Cases D and E, the most highly reinforced, debonding does not occur, and the collapse mode is governed primarily by material crushing at the crown.

Table 2. The considered arches

Case	FRP width b_f(cm)	Collapse Load (N)
A	Unreinforced	450
B	1.25	3560
C	2.5	4520
D	5	6580
E	10	7250

In performing the numerical analysis of Case A, the applied load was incremented until numerical convergence was no longer achievable. The last value obtained (F = 450N) coincides with the actual collapse load determined experimentally, thus highlighting the perfect agreement between the model's prediction and the experimental results. Furthermore, the model accurately describes the observed collapse mechanism, as shown in Fig. 5.

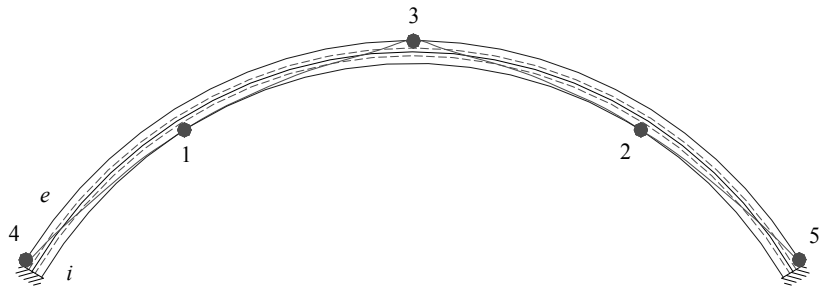

Figure 5 : Line of thrust and five hinge collapse mechanism obtained by numerical simulation.

For the reinforced arches (Cases B, C, D), instead, the applied load has been incremented up to the value that resulted in collapse experimentally, and the numerical values of f_b (Fig. 6a) and ε_m (Fig. 6b) corresponding to such a load value then determined.

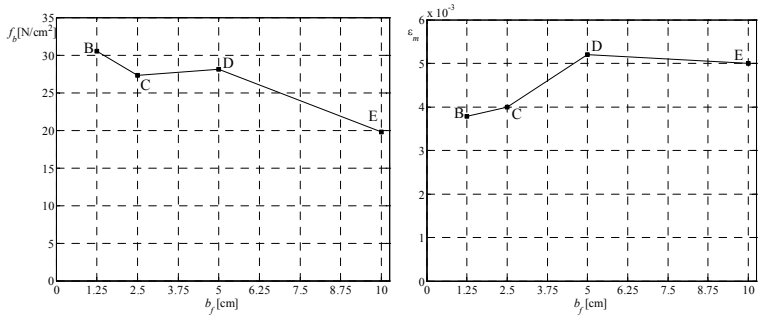

a) b)

Figure 6 : Values of: a) stress at the interface, b) masonry maximum compressive deformation reached at collapse in the four cases considered (B, C, D, E) as a function of the amount of fiber b_f.

Fig. 6 shows that the numerical results are consistent with the collapse mode exhibited in each case. Indeed, Case B, in which premature failure by debonding occurs, yields larger values of f_b than the other cases, while the value ε_m is quite contained. Conversely, for Case E, in which crushing failure occurs, f_b is less important, while ε_m is more significant. Moreover, in Case C, which represents an intermediate situation (i.e. with both debonding and crushing), the values of f_b and ε_m fall within the range defined by the two previously discussed Cases. Lastly, in Case D, in which crushing prevails, although the value of f_b is relatively large, ε_m reaches its maximum value.

4 CONCLUSIONS

A numerical model for studying FRP-strengthened masonry arches has been developed and implemented into a finite element procedure. The implemented code allows for analyzing the structural response of arches with various geometries and restraints under very general load conditions. The model assumption that masonry is a no-tension material with limited compressive strength enables capturing collapse failure involving masonry cracking and crushing. Although the current model does not allow for post-debonding analyses, possible premature failures due to the FRP detachment are revealed by the stress values at the FRP-masonry interface, as evaluated by means of a simple procedure.

As the limited amount of data currently available does not permit identifying values of $f_{b,lim}$ and $\varepsilon_{m,lim}$, the comparisons between numerical and experimental results have been discussed from a qualitative standpoint alone. Nonetheless, the predictions of the proposed model reveal to be quite consistent with the experimental results, thus encouraging further development.

REFERENCES

Ascione L., Feo L., Fraternali F. 2005. Load carrying capacity of 2D FRP/strengthened masonry structures. *Composites: Part B,* 36, p. 619-626.

Bakis C.E., Bank L.C., Brown V.L., Cosenza E., Davalos J.F., Lesko J.J., Machida A., Rizkalla S.H., Triantafillou T.C. 2002. Fiber-reinforced polymer composites for construction-State-of-the-art review. *ASCE Journal of composites for construction*, Vol.6, n°2, May 1.

Briccoli Bati S. and Rovero L. 2000. Use and abuse of the FRP (fiber reinforced polymer) for consolidation of masonry structures. *ICCE/7, 7th Annual International conference on composites engineering*, Denver, Colorado, July 2-8, pp. 753-754.

Briccoli Bati S., Rovero L., Tonietti U. 2004. Strengthening of masonry arches with composites materials. *1st International Conference on innovative materials and technologies for constructions and restorations*, Vol.2, Lecce, Italy, June 6-9, pp. 386-402.

Drosopoulos G.A., Stavroulakis G.E., Massalas C.V. 2007. FRP reinforcement of stone arch bridges: Unilateral contact models and limit analysis. *Composites: Part B,* 38, p. 144-151.

Heyman, J. 1982. *The Masonry Arch*. John Wiley.

Lucchesi, M., Padovani, C., Zani, N. 1996. Masonry-like solids with bounded compressive strength. *International Journal of Solids and Structures* 33, pp. 1961-1994.

Luciano R., Marfia S., Sacco E. 2002. Reinforcement of masonry arches by FRP materials: experimental tests and numerical investigations. *International Conference in composites for infrastructures, ICCI2002*, San Francisco, June 10-12.

Pintucchi B. and Zani N. Effects of material and geometric non-linearities on the collapse load of masonry arches. (in preparation).

Triantafillou T.C. 1998. Strengthening of masonry structures using epoxy-bonded FRP laminates. *Journal of composites for construction*, Vol.2, n°2, May, pp.96-104.